

**Universitat de Lleida**

Document downloaded from:

<http://hdl.handle.net/10459.1/67803>

The final publication is available at:

<https://doi.org/10.1111/aab.12484>

Copyright

(c) Association of Applied Biologists, 2019

**Running title:** UAV's imagery for phenotyping forest genetic trials

**Title:** Using UAV-based multispectral, RGB and thermal imagery for phenotyping of forest genetic trials: a case study in *Pinus halepensis*

F. Santini<sup>a</sup>, S. C. Kefauver<sup>b,c</sup>, V. Resco de Dios<sup>a</sup>, J.L. Araus<sup>b,c</sup>, J. Voltas<sup>a\*</sup>

<sup>a</sup> Department of Crop and Forest Sciences – AGROTECNIO Center, University of Lleida, Av. Alcalde Rovira Roure 191, E-25198 Lleida, Spain.

<sup>b</sup> Integrative Crop Ecophysiology Group, Plant Physiology Section, Faculty of Biology, University of Barcelona, Av. Diagonal 643, E-08028 Barcelona, Spain

<sup>c</sup> AGROTECNIO Center, Av. Alcalde Rovira Roure 191, E-25198 Lleida, Spain.

\* Corresponding author: Jordi Voltas

Department of Crop and Forest Sciences – AGROTECNIO Center

ETSEA-University of Lleida

Av. Alcalde Rovira Roure 191

E-25198 Lleida, Spain

tel. +34 973 702855

e-mail: [jvoltas@pvcf.udl.cat](mailto:jvoltas@pvcf.udl.cat)

## Summary

The assessment of genetic differentiation in functional traits is fundamental towards understanding the adaptive characteristics of forest species. While traditional phenotyping techniques are costly and time-consuming, remote sensing data derived from cameras mounted on UAVs (unmanned aerial vehicles) provide potentially valid high-throughput information for assessing morphophysiological differences among tree populations. In this work, we test for genetic variation in vegetation indices and canopy temperature among populations of *Pinus halepensis* as proxies for canopy architecture, leaf area, photosynthetic pigments, photosynthetic efficiency and water use. The inter-population associations between vegetation properties and above-ground growth (stem volume) were also assessed. Three flights (July-2016, November-2016 and May-2017) were performed in a genetic trial consisting of 56 populations covering a large part of the species range. Multispectral (visible and near infrared wavelengths), RGB (red, green, blue) and thermal images were used to estimate canopy temperature and vegetation cover (VC) and derive several vegetation indices. Differences among populations emerged consistently across flights for vegetation cover and vegetation indices related to leaf area, indicating genetic divergence in crown architecture. Population differences in indices related to photosynthetic pigments emerged only in May-2017 and were probably related to a contrasting phenology of needle development. Conversely, the low population differentiation for the same indices in July-2016 and November-2016 suggested weak inter-population variation in the photosynthetic machinery of mature needles of *P. halepensis*. Population differences in canopy temperature found in July-2016 were indicative of variation in stomatal regulation under drought stress. Stem volume correlated with indices related to leaf area (positively) and with canopy temperature (negatively), indicating a strong influence of canopy properties and stomatal conductance on above-ground growth at the population level. Specifically, a combination of vegetation indices and canopy temperature accounted for about 60% of population variability in stem volume of adult trees. This is the first study to propose UAV remote sensing as an effective tool for screening genetic variation in morphophysiological traits of adult forest trees.

**Key-words:** Aleppo pine, common garden experiment, functional traits, leaf area, population differentiation, spectral imaging, stem volume, stomatal regulation

## **Introduction**

The analysis of genetic variation in functional traits is fundamental towards understanding the adaptive properties of forest trees and to forecast responses to ongoing environmental changes (Bussotti et al., 2015). Genetic trials are well suited for assessing adaptive variation among tree populations (Mátyás, 1996). Traits such as growth or phenology are typically evaluated in field trials (i.e. common garden experiments), occasionally in conjunction with functional characteristics such as reproductive effort (Santos-del-Blanco et al., 2013), stem hydraulic properties or leaf gas exchange (Klein, 2014). However, large-scale phenotyping of forest genetic trials is methodologically challenging. The need to implement costly and time-consuming techniques is often a limitation for extensive phenotyping of adult trees (Ludovisi et al., 2017). This constraint impacts negatively on the number of populations and traits that can be evaluated simultaneously, and may lead to the inadequate coverage of the suite of adaptive and plastic responses that are typical of forest species (Savolainen et al., 2007).

Conversely, high-throughput phenotyping tools have been developed in plant sciences that enable a straightforward evaluation of hundreds of individuals with reduced economic and time costs (Großkinsky et al., 2015; Lobos et al., 2017). In this regard, remote sensing imagery acquired with unmanned aerial vehicles (UAVs) allows for an efficient morphophysiological characterization of a large number of experimental units (Tattaris et al., 2016). UAV-mounted multispectral and RGB (red, green, blue) cameras can detect light reflectance variation, while thermal cameras estimate canopy temperature (Sankaran et al., 2015). Several vegetation indices can be derived through RGB and multispectral sensors, providing information about canopy properties, leaf area, leaf chemical composition and photosynthetic efficiency (Casadesús et al., 2007; Fahlgren et al., 2015; Xue & Su, 2017). Specific associations between functional traits and vegetation indices have been long established and are well described in the scientific literature (e.g., Roberts et al., 2016; Xue & Su, 2017). These indices have been shown to be good predictors of physiological performance and productivity in field crops (Yu et al., 2016; Gracia-Romero et al., 2017) and forest species (Hernández-Clemente et al., 2012). Moreover, thermal imagery provides information on canopy temperature that is linked to transpiration and plant water status (Costa et al., 2013; Gonzalez-Dugo et al., 2013). UAV-based remote sensing allows for high spatial resolution imagery and, therefore, is a promising tool for forest tree phenotyping. Indeed, UAVs are already being used for different purposes in forestry, including inventories, species classification, spatial gaps quantification, fire monitoring, and pest and pathogen mapping (Tang & Shao, 2015; Torresan et al., 2017). To date, however, the potential of UAVs as a tool

for remote sensing assessments of intra-specific differentiation in phenotypic traits remains untested in adult forest trees (Ludovisi et al., 2017).

In this work, we characterise the extent of inter-population differences in functional traits related to canopy architecture and tree physiology through high-resolution remote sensing data obtained in a common garden experiment. We focus on Aleppo pine (*Pinus halepensis* Mill.), the most widespread conifer of the Mediterranean basin. Aleppo pine is a drought-avoidant species that is prevalently distributed in the central-western part of the Mediterranean basin, where it provides important ecosystem services and it is widely used for reforestation (Pausas et al., 2004; Choury et al., 2017). Due to its circum-Mediterranean distribution range, *P. halepensis* can be found under contrasting growing conditions which, coupled with a complex history of demographic contractions and expansions, have shaped current intra-specific patterns of genetic variation (Serra-Varela et al., 2017). In particular, population differentiation has been reported in this species for many key traits, including aerial growth (Schiller & Atzmon, 2009; Voltas et al., 2018), phenology (Klein et al., 2013), water uptake patterns (Voltas et al., 2015), hydraulic conductivity (Tognetti et al., 1997) and reproductive effort (Climent et al., 2008).

We hypothesised that (i) morphophysiological properties related to drought resistance and inferred through remote sensing data should vary among populations of *P. halepensis* (Otieno et al., 2005; Voltas et al., 2008), and (ii) population differentiation in such properties can explain variation in above-ground growth. To test these hypotheses, we used UAV imagery as high-throughput phenotyping tool in a genetic trial of this conifer composed of adult individuals. More specifically, we sought to (i) assess genetic variation in canopy architecture, leaf area, photosynthetic pigments and stomatal regulation in three consecutive seasons of the year (summer, autumn, spring) as indicated by differentiation in vegetation cover, vegetation indices and canopy temperature, and (ii) explore the associations between ecophysiological properties and above-ground growth (stem volume) at the intra-specific level.

## **Material and Methods**

### **Study site and plant material**

The study was performed in a common garden experiment of *P. halepensis* located in Altura (39°49'29"N, 00°34'22"W, 640 m a.s.l.; Castellón province, eastern Spain, Fig. 1A; Fig. S1). The site has a mean annual temperature of 13.8°C and mean annual precipitation of 652 mm,

of which 19% falls in summer (June to August). These climatic conditions are representative of the average values of the species' distribution range (Fig. 1B). Seeds were collected in 1995 in 56 natural populations of *P. halepensis* covering most of the range of the species (Supporting Information, Table S1, Fig. S1). Seeds were harvested from 20-30 trees that were spaced at least 100 m apart and planted in a forest nursery in Spain. In 1997, one year old seedlings were planted systematically (2.5 m spacing within rows and columns) at the study site. Four seedlings from each provenance were planted in experimental units consisting of linear plots (Fig. 1C). Four replicates were established following a Latinised row-column design (John & Williams, 1998) for a total of 896 seedlings (16 per population) tested in the trial. Each row had approximately 70 m long corresponding to seven plots and four trees per plot. In 2010 (at age 13), height and diameter at breast height were registered per tree, and data were used to calculate the stem volume over bark ( $V_{ob}$ ) following the equation:

$$V_{ob} = (\pi/12) \times D^2 \times H \quad (1)$$

where  $D$  is the diameter at breast height and  $H$  is the tree height, assuming the stem to be conical.  $V_{ob}$  was used as surrogate of total above-ground biomass (Reinhardt et al., 2006). In 2016, survival was recorded at the plot level with a ground-based visual inspection.

#### Aerial data collection

Aerial images of the trial (Fig. 1A) were obtained through a UAV (Mikrokopter OktoXL, Moormerland, Germany) flying under remote control at around 100 m of altitude. Three different cameras were mounted down-looking on the UAV in consecutive flights done during the same day. First, a multispectral camera (MCA12; Tetracam Inc., Chatsworth, CA, US) was operated which simultaneously captured 15.6-megapixel images in 10 wavelengths ( $450 \pm 40$ ,  $550 \pm 10$ ,  $570 \pm 10$ ,  $670 \pm 10$ ,  $700 \pm 10$ ,  $720 \pm 10$ ,  $840 \pm 10$ ,  $860 \pm 10$ ,  $900 \pm 20$ ,  $950 \pm 40$  nm) in the visible and near infrared (NIR) regions of the spectrum. An extra sensor, incorporated in the multispectral camera, registered incident light (IL), hence resulting in real-time calibration of reflectance for each of the 10 wavelength images recorded during a flight. These images were pre-processed with the Tetracam PixelWrench software (Tetracam Inc., Chatsworth, CA, US) in order to correctly align the images. To ensure high quality image registration in the pre-processing stage, care was taken to keep forward motion limited to less than  $5 \text{ m s}^{-1}$  in the UAV flight. The accuracy of the reflectance measurements of the

multispectral camera was evaluated in a previous study using the same sensor and UAV platform (Kefauver et al., unpublished data). Particularly, the camera records were compared with the spectral reflectance of the same plots of a durum wheat trial measured with an ASD field spectrometer (ASD, Boulder, CO, USA), resulting in simple correlations varying between 0.95 and 0.97 for the 10 wavelengths. Second, a Mirrorless Interchangeable Lens Camera (MILC) with an image sensor size of  $17.3 \times 13.0$  mm was used for the acquisition of RGB images (Lumix GX7; Panasonic, Osaka, Japan). Images were taken at 16-megapixel resolution using a 20-mm focal length. Third, a FLIR (Tau2 640; FLIR Systems, Nashua, NH, USA) camera carrying a vanadium oxide uncooled microbolometer equipped with a TEAX ThermalCapture module (TEAX Technology, Wilnsdorf, Germany) was employed for the acquisition of thermal images. The temperature measurements obtained with the UAV-mounted thermal camera for a vegetated, a completely white and a completely black surface were compared with ground-based measurements of the temperature recorded with an infrared thermometer, resulting in a correlation of 0.96.

The spatial resolution of the photographs was *ca.* 1, 2.7 and 5.4 cm per pixel in the case of RGB, multispectral and thermal cameras, respectively. Images were taken at the rate of one every 5 s for the RGB and multispectral cameras, resulting in *ca.* 120 pictures obtained per flight (*ca.* 10 minutes long). In the case of the thermal camera, images were extrapolated from a video with a frame (image) rate of 20 images per second. Flights were done in summer (26 July 2016), autumn (17 November 2016) and spring conditions (25 May 2017) in two consecutive growing seasons, following a trajectory designed to spatially cover the entire study site (Fig. 1A). The flights took place at noon and with a completely clear sky to minimize shadow effects and changes in light intensity. Environmental and sun conditions at the moment of the flights are reported in Table 1.

### Image processing

For each flight the raw multispectral, RGB and thermal images were combined to produce orthomosaic images. The Agisoft PhotoScan Professional software (Agisoft LLC, St. Petersburg, Russia) was employed for this purpose using a variable number of images with at least 80% overlap. Nine orthomosaics resulted from this process (i.e. three orthomosaics per flight – one multispectral, one RGB and one thermal – and three flights) which were used for subsequent analyses. The open-source image analysis platform Fiji (Schindelin et al., 2012) was used to identify and crop single linear plots (corresponding to four trees) in each

orthomosaic (Fig. 1C, 1D). In total, 224 single images (corresponding to the experimental units of the trial) were obtained for each flight and imagery (multispectral, RGB and thermal).

### Multispectral indices

A number of vegetation indices (VIs) were derived from multispectral data based on the reflectance at 10 wavelengths (Table 2). The VIs were calculated for each pixel using a macro code in the Fiji platform, and a mean value per plot was obtained afterwards. The indices are linked to different functional traits in relation to the wavelengths used for calculations. Several indices (based on red and NIR reflectance) are mainly linked to leaf area, being relatively insensitive to leaf chlorophyll content (Roberts et al., 2016; Xue & Su, 2017). Specifically, these are:

- the Normalized Difference Vegetation Index (NDVI), which is broadly used and based on the reflectance in red and NIR wavelengths (Rouse et al., 1974);
- the Enhanced Vegetation Index (EVI, Huete et al., 2002), which is an optimized NDVI-based index developed to minimize the noise due to atmospheric reflectance;
- the Renormalized Difference Vegetation Index (RDVI, Roujean & Breon, 1995);
- the Optimized-Soil Adjusted Vegetation Index (OSAVI, Rondeaux et al., 1996). RDVI and OSAVI were both proposed to minimize the effect of the background (i.e. soil) reflectance.

Alternatively, other indices include the reflectance in the green wavelengths and are negatively related to leaf chlorophyll content. These indices are:

- the Modified Chlorophyll Absorption Ratio Index (MCARI, Daughtry et al., 2000);
- the Transformed Chlorophyll Absorption Ratio Index (TCARI, Haboudane et al., 2002).

However, these indices are also sensitive to background reflectance and can be influenced by differences in leaf area (Daughtry et al., 2000). A better estimation of leaf chlorophyll content can be obtained by correcting TCARI by an index that accounts for leaf area. In this regard, an index related to chlorophyll content and free of the effect of leaf area is:

- the ratio between TCARI and OSAVI (TCARI/OSAVI, Haboudane et al., 2002; Zarco-Tejada et al., 2004).

Alternative indices related to other leaf pigments and water content are:

- the Anthocyanin Reflectance Index 2 (ARI2, Gitelson et al., 2001);
- the Carotenoid Reflectance Index 2 (CARI2, Gitelson et al., 2002);

- the Water Band Index (WBI, Peñuelas et al., 1993), which is related to the water content of leaves.

It must be taken into account that the values of vegetation indices, when calculated at the whole-plot level, arise as the combination of vegetation characteristics and vegetation cover (VC, or percentage of pixels containing vegetation). Phenotypic variation in vegetation properties within the canopy that influence such indices could be partly masked by phenotypic variation in crown size (i.e. VC). To overcome this issue, we applied a filter to distinguish between pixels containing vegetation and pixels containing soil. The filter was based on the NDVI index, which was first developed to discriminate between vegetation and other surfaces (Richardson & Wiegand, 1977). The reflectance in NIR wavelengths of pure soil surface is slightly higher than the reflectance in red wavelengths, resulting in NDVI values of 0-0.2. Conversely, the NDVI is higher in vegetation surfaces, due to the high absorption in red wavelengths and the high reflectance in NIR wavelengths. Based on this, we applied an NDVI threshold of 0.5, considering as vegetated pixels those showing  $NDVI > 0.5$  (Fig. 1E). The multispectral VIs were recalculated using vegetated pixels as to be representative of differences in the properties of the vegetation, excluding differences in VC.

### RGB vegetation indices

While multispectral indices have been used for long time as proxies of specific vegetation characteristics, RGB imagery has been only recently proposed as a low-cost alternative for plant phenotyping (Kefauver et al., 2017; Gracia-Romero et al., 2018). Indeed, a clear association with specific phenotypic traits is still lacking in the scientific literature for many RGB-derived VIs. As potential alternative to multispectral indices, several VIs based on colour properties and related to the degree of greenness of the image were retrieved from RGB images (Casadesús et al., 2007), as described below.

RGB images corresponding to single experimental units (Fig. 1C) were analysed using a version of the Breedpix 2.0 software implemented as a plug-in within Fiji (Casadesús & Villegas, 2014). This software calculates VIs on single pixels in each image and then provides a mean value per plot. In order to evaluate a wide range of RGB indices, three different models representing the colour space in different ways were considered to derive such indices. In the HSI (Hue, Saturation, Intensity) model (Judd, 1940), *Saturation* and *Intensity* describe the grade of purity of the colour and the light intensity, respectively, while *Hue* describes the colour itself in the form of an angle between  $0^\circ$  and  $360^\circ$ , where  $0^\circ$  means red,

60° means yellow, 120° means green and 180° means cyan. Derived from *Hue*, the Green Area (GA) index is defined as the percentage of green pixels in the image (*Hue* range from 60° to 180°). Two alternative models to HSI (CIELab and CIELuv) are defined according to the International Commission of Illumination (<http://www.cie.co.a>). In the CIELab model, the  $a^*$  component represents the green to red range, with a more positive value representing a purer red, and a more negative value indicating a greener colour. The  $b^*$  component defines the blue to yellow range, where more positive values are closer to a pure yellow and more negative ones are closer to pure blue. In the CIELuv model, the colour space is represented as a Cartesian system with two coordinates,  $u^*$  and  $v^*$ . The visible spectrum starts with blue at the bottom of the space, moving through green in the upper left and to red in the upper right. It must be noted that the RGB-derived VIs described above are not calculated based on reflectance in specific wavelengths; instead, they are descriptors of the colour space. Alternatively, the RGB images can be used to calculate additional indices based on the reflectance in different wavelengths of the visible spectrum: the normalized green red difference index (NGRDI), which is based on the reflectance in the red and green bands, and the triangular greenness index (TGI), which includes also the reflectance in blue bands (Table 2).

The NDVI-based filter that was applied to the multispectral images to remove non-vegetated pixels could not be applied to RGB images due to the different type of imagery. For this reason, only whole plot RGB-indices (which includes vegetated and non-vegetated pixels) could be calculated.

### Thermal images

Thermal images were used to retrieve information on canopy temperature. Since average plot temperature is related to vegetation cover, a filter based on an automatic Otsu's classification (Otsu, 1979) was applied to the thermal images in order to discriminate between vegetated and non-vegetated pixels. The algorithm assumes that images contain two classes of pixels (ground and vegetation) and automatically finds an optimum threshold (temperature) to separate between classes. Based on the pixels classified as "vegetation", a second estimation of vegetation cover was obtained ( $VC_T$ ); these pixels were later used to derive the mean canopy temperature of each plot.

## Statistical analyses

First, we evaluated the presence of significant inter-population variation in vegetation indices, vegetation cover and canopy temperature (as proxies of differentiation in canopy architecture, leaf area, photosynthetic pigments and water use) for each flight independently. Afterwards, the association between UAV-based vegetation characteristics and stem volume was tested. Prior to the analyses, plots having three dead trees were discarded, since dead trees could strongly bias the performance of neighbouring trees due to reduced competition. These plots represented only 2% of the total number of plots and showed strongly deviating values of VIs. Also, plots at the edges of the trial might have shown values influenced by reduced competition (i.e. border effects). Nevertheless, these plots (7%) were kept in the analyses because they did not show up as outliers. In total, 219 plots (corresponding to 818 trees) were used for statistical analyses.

### *Analysis of variance of individual traits*

Stem volume, vegetation indices, vegetation cover and canopy temperature at the plot level were subjected to analysis of variance (ANOVA) for linear mixed-effects models in order to test for population differences in UAV-based phenotypic traits. ANOVAs were fitted independently for each flight date. Stem volume records were log-transformed prior to ANOVA to achieve homoscedasticity of residuals. ANOVAs consisted of fixed population, replicate and column terms and random column by replicate interaction and row nested to replicate terms.

For those indices showing significant population differences, Spearman's rank correlations involving population means were calculated across flights to check for consistency in population ranking.

### *Relationships between vegetation indices*

The use of RGB-derived vegetation indices is relatively recent compared to multispectral imagery. While multispectral VIs based on specific reflectance bands have been linked to particular phenotypic traits (Roberts et al., 2016; Xue & Su, 2017), few literature is available for many RGB indices considered in this work. In order to compare the information retrieved by RGB and multispectral VIs, simple correlations were calculated across populations. Moreover, the populations' least square means of the different vegetation indices and of canopy temperature were subjected to Principal Component Analysis (PCA) for each flight

date and index type independently (multispectral, multispectral corrected by vegetation cover and RGB-derived), and PCA loadings were plotted to summarise the information contained in the different variables.

#### *Population-level associations between stem volume and UAV-based imagery information*

When significant population effects were detected, simple correlations involving log-transformed stem volume and VIs, vegetation cover or canopy temperature were calculated for each flight date using population means. This analysis aimed at indirectly test for the effects of a number of functional traits related to UAV imagery (canopy architecture, leaf area, photosynthetic pigments and water use) on population differentiation in above-ground growth. We assumed that the ranking of populations for stem volume remained stable at adult stage (age > 10 in *P. halepensis*), as reported elsewhere for pines (Li & Wu, 2005). Hence, growth data obtained in 2010 (at age 13) was compared with UAV imagery records.

The variability in stem volume across populations explained by vegetation properties (vegetation cover, vegetation indices and canopy temperature) was assessed through stepwise linear regression in July-2016 and May-2017. This analysis was not performed in November-2016 due to the lack of reliable VIs estimation (see “Methodological limitations” in the Discussion section). The analyses were carried out using a bidirectional (forward and backward) elimination procedure based on input and output  $F$  probabilities of 0.15. The goodness of fit was evaluated considering the coefficient of determination ( $R^2$ ) and the root-mean-square error (RMSE) of the regression. Different models were tested, either considering one particular family of VIs (RGB-derived indices, multispectral indices measured in either whole plots or vegetated pixels) or, alternatively, combining RGB-derived and multispectral indices. Vegetation cover was also included in the regressions involving multispectral indices. In the case of July-2016, the analyses were also performed including canopy temperature in the models (canopy temperature was not included in May-2017 because of lack of population differentiation for this trait).

## **Results**

### Population variation in UAV-based imagery information and stem growth

The population term in the ANOVAs was significant ( $P < 0.05$ ) for many VIs related to different functional traits and, also, for log-transformed stem volume (log-Vob, Table 3).

Average population values of VIs are reported in Supporting Information for each flight (Table S2).

Most multispectral indices obtained at the plot level showed significant differences among populations, with the exceptions of TCARI/OSAVI, which was non-significant regardless of flight date. However, significant population differences in vegetation cover (VC), which may influence the variation in multispectral VIs, were found regardless of flight date (Table 3). Population means for VC varied between 52% and 69% in July-2016, between 51% and 67% in November-2016, and between 53% and 66% in May-2017. VC estimates were consistent across flights, as indicated by significant rank correlations and low absolute differences (<10%) at the plot level. Once the multispectral VIs were recalculated considering vegetated pixels only, significant population differences emerged for indices related to leaf area (i.e. NDVI, OSAVI, RDVI, EVI, MCARI and TCARI) across flight dates (Table 3). For those indices related to needle pigment composition (i.e. TCARI/OSAVI, ARI2 and CRI2) and water content (i.e. WBI), significant population differences were found only in May-2017. In the case of RGB-derived VIs, population differences were found in July-2016 (with the exception of TGI and *Intensity*) and May-2017. Population differentiation was also observed in November-2016, but only for three indices ( $a^*$ ,  $u^*$  and GA).

For thermal data, we could not distinguish between soil and vegetation pixels in November-2016 owing to small differences in temperature between soil and canopy. For this particular flight date, the mean temperature of the whole plot was used as response variable in the ANOVA. In July-2016 and May-2017,  $VC_T$  was significantly correlated with VC at the plot level, even if  $VC_T$  estimates were usually higher. Based exclusively on vegetated pixels, the ANOVA revealed population differences in canopy temperature only in July-2016, while population differentiation in temperature was not significant based on whole-plot (in November-2016) or vegetated pixels (in May-2017, Table 3).

For those indices showing population variation in different flights, significant Spearman correlations across flight dates indicated consistent population rankings (Table S3). Population ranking for vegetation cover was also consistent across flights.

#### Relationships between vegetation indices

The relationships between RGB-derived indices and multispectral indices at the population level provided information regarding the functional traits that could be potentially inferred by RGB imagery. Specifically, most RGB VIs were significantly correlated with the suite of

multispectral indices related to leaf area obtained either for whole plots or for vegetated pixels only (Supporting Information, Table S4, S5, S6). Exceptions were TGI and *Intensity* (in July-2016) and *Hue* (in May-2017). Correlations between RGB-derived indices and multispectral indices related to pigment content (e.g. TCARI/OSAVI as indicator of needle chlorophyll content) were poorer and less consistent across flight dates (Supporting Information, Table S4, S5, S6). As an exception, TGI and *Intensity* were significantly correlated ( $r \geq 0.55$ ) with TCARI/OSAVI in May-2017. Most RGB-derived and multispectral indices were also significantly correlated with VC across flight dates at the population level (Table 4).

The PCA loadings provided insights into the existing relationships among vegetation indices (see Fig. 2 for the case of July-2016). For multispectral data, the relationships between indices were quite consistent across flights (with the exception of November-2016; results not shown), regardless of whether they were calculated on whole plots (Fig. 2A) or on vegetated pixels only (Fig. 2B). The indices related to leaf area (i.e., NDVI, RDVI, OSAVI, EVI, MCARI and TCARI) grouped together in the plot of loadings, opposite to canopy temperature (Fig. 2A; Fig. 2B). In turn, TCARI/OSAVI (informative of chlorophyll content) and WBI (of leaf water content) were negatively associated and unrelated to most other indices. Finally, ARI2 and CRI2 (informative of anthocyanins and carotenoid leaf content respectively) were poorly explained by the first two PCA dimensions. For RGB-derived indices, two patterns of associations could be distinguished regardless of flight date (see Fig. 2C for the case of July-2016). TGI and *Intensity* clustered together, being independent of the rest of indices, which in turn were tightly associated among them.

#### Population-level associations between stem volume and UAV-based imagery information

VIs often correlated significantly with log-Vob across populations (Table 4). The highest correlations were found in July-2016 and involved multispectral indices related to leaf area estimated on vegetated pixels ( $r \geq 0.50$ , Table 4). Significant correlations were often observed also in November-2016, regardless of index type. In May-2017, correlations with log-Vob were similar across different classes of indices (multispectral or RGB), with the exception of multispectral indices related to leaf pigments and water content, which resulted poorly correlated with log-Vob (Table 4). Vegetation cover was significantly correlated with log-Vob in July-2016, November-2016 and May-2017 ( $r \geq 0.27$ ).

Canopy temperature was negatively correlated with log-Vob across populations in July-2016 (Fig. 3). Also, canopy temperature was negatively and significantly correlated with

multispectral indices related to leaf area as measured on vegetated pixels (i.e. NDVI, OSAVI, RDVI, EVI;  $r = \leq - 0.52$ ). To account for the effect of leaf area on the relationship between canopy temperature and log-Vob, partial correlations controlling for such indices (NDVI, OSAVI, RDVI or EVI) were calculated across populations. These correlations were also significant ( $r \leq - 0.49$ ).

Over 60% of the variability in growth was explained by a combination of vegetation properties. The best stepwise regression model of population differences in log-Vob was obtained in May-2017, and included a combination of multispectral and RGB indices measured on vegetated pixels ( $R^2 = 0.63$ , RMSE = 0.198, Table 5). Alternative regressions based on combinations of multispectral VIs showed lower  $R^2$  and higher RMSE. In July-2016, the best predictive model was obtained combining canopy temperature and a multispectral index related to leaf area such as EVI ( $R^2 = 0.60$ , RMSE = 0.278). In general, regressions including canopy temperature were better predictors of log-Vob in July-2016, regardless of VI. Indeed, canopy temperature alone explained 57% variability among populations.

## **Discussion**

The potential of UAV-derived remote sensing data as phenotyping tool is widely acknowledged in plant sciences (Sankaran et al., 2015). In this work, we have proposed a straightforward strategy for UAV-based characterisation of population differentiation in key functional traits of a forest tree species. Although several UAV-based applications have been described in forest sciences (e.g., Hernández-Clemente et al., 2012; Tang & Shao, 2015; Torresan et al., 2017), this is to the best of our knowledge the first attempt to apply high-throughput phenotyping techniques based on aerial imagery in forest genetic trials comprising adult trees.

The extent of population differentiation in vegetation indices and canopy temperature as proxies of functional traits

Many multispectral indices measured on the whole plot varied among populations, suggesting genetic differentiation in several functional traits. However, these indices were also sensitive to variations in vegetation cover, which could have determined population differences for these indices (Purevdorj et al., 1999). In particular, the confounding effect of vegetation cover on plot-level multispectral indices may explain the lack of population differentiation for some

indices (e.g. NDVI, TCARI/OSAVI or CRI2), otherwise relevant when considering only vegetated pixels. Indeed, multispectral indices measured on vegetated pixels are free of changes in vegetation cover (i.e. canopy width), being representative of variations in other canopy properties (Xue & Su, 2017). In general, however, multispectral indices showed similar relationships when measured on the whole plot or on vegetated pixels, as revealed by PCAs.

NDVI-related multispectral indices (i.e. OSAVI, RDVI, EVI, MCARI and TCARI) measured on vegetated pixels showed significant population variation and similar population ranking across seasons, suggesting the existence of constitutive population differences in within-canopy characteristics in *P. halepensis*. As already stressed, these indices have been long used as indicators of variation in leaf area (e.g., Roberts et al., 2016; Xue & Su, 2017) also at the individual tree level (Berni et al., 2009). These evidences point to the existence of population differentiation in the number or area of needles per pixel, thereby indicating differences in canopy density as previously reported for other pine species (McRady & Jokela, 1996). Population differentiation was also found for vegetation cover across flights. Canopy structural properties such as branches' surface and distribution can impact on crown shape and concur with leaf area to determine differentiation in vegetation cover (Baldwin et al., 1997; Weiskittel & Maguire, 2006). These findings suggest complex patterns of canopy architecture among populations of *P. halepensis*. Canopy structural properties have significant implications in many physiological traits, including foliage surface exposure and total radiation absorption (Niinemets, 2010). Reduced leaf area in some populations may also be associated to drought resistance as the result of a lower transpiring surface (Eamus et al., 2000; Otieno et al., 2005).

MCARI and TCARI take into account the reflectance in the green spectral region at 550 nm, revealing also potential differences in chlorophyll content of leaves (Daughtry et al., 2000). However, MCARI and TCARI were probably indicative of differences in leaf area, rather than in chlorophyll content, according to population differentiation observed across flight dates. This is because significant population differences emerged only in spring for TCARI/OSAVI, which is an index specifically informative of leaf chlorophyll content (Zarco-Tejada et al., 2004; Wu et al., 2008). In this regard, MCARI and TCARI (but also EVI, which includes reflectance in the blue band) showed lower, although significant, Spearman's correlations across flights compared to indices that consider only the reflectance in red and NIR (i.e. NDVI, OSAVI and RDVI). Other indices related to carotenoid, anthocyanin or water content in leaves also showed significant population variation in spring if calculated on

vegetated pixels, which reinforces the existence of population differences in needle biochemical composition early in the growing season. Contrasting photosynthetic spring recovery or different phenology of needle emergence could explain variation in pigments and water content among pine populations in spring (Wong & Gamon, 2015). The scarce information available on needle phenology in *P. halepensis* indicates that new needles draw apart from the shoot in mid-spring, reaching the final size only in full summer (Weinstein, 1989). This evidence is consistent with our findings and points to differential needle development among populations of *P. halepensis*. On the other hand, our results indicate a lack of genetic differentiation in the photosynthetic apparatus (i.e. photosynthetic pigments) of mature needles of *P. halepensis*, which is consistent with a previous work carried out in the same trial suggesting weak differentiation in photosynthetic capacity among populations of *P. halepensis* (Voltas et al., 2008).

In recent years, RGB imagery has been proposed as cost-effective alternative to multispectral records for plant phenotypic characterization (Kefauver et al., 2017; Gracia-Romero et al., 2018). RGB imagery has limited possibilities for studying physiological processes such as gas exchange or leaf biochemistry (Großkinsky et al., 2015). However, RGB-derived vegetation indices can be easily obtained from standard cameras and are suitable for studying the morphological characteristics of the vegetation. In this work, two distinct groups of RGB indices provided contrasting information on functional traits of *P. halepensis* populations. The first group included the *Intensity* parameter, which is indicative of the brightness of the picture, and the TGI index, which has been related to leaf chlorophyll content (Hunt et al., 2011). The population differentiation in TGI in spring indicates variability in chlorophyll content in needles among populations of *P. halepensis* during spring, as suggested also by some multispectral indices. However, the tight association of TGI with *Intensity* cannot exclude a preponderant effect of pictures' brightness on TGI variation, making the interpretation of this index difficult. Conversely, a second group of indices showed significant population variation and consistent genetic ranking across flights. Most of these indices are related to the overall "greenness" of the image and have been linked to leaf area in field crops (Hunt et al., 2005; Casadesús & Villegas, 2014). In this regard, the strong and consistent correlations found at the population level between RGB and multispectral indices related to leaf area suggest that RGB indices are indicative of population differences in number of needles, in their total surface, or in both factors simultaneously. Our results suggest that RGB imagery can be a (partial) alternative to multispectral indices for tree

phenotyping with UAV, as already proposed for herbaceous crops (Casadesús et al., 2007; Kefauver et al., 2017; Gracia-Romero et al., 2018).

The population differentiation in canopy temperature observed in summer is indicative of divergence in transpiration rate (Gonzalez-Dugo et al., 2013). Disentangling the effects of total leaf area and stomatal conductance on canopy temperature is complex, and canopy temperature was found to be correlated with vegetation indices related to leaf area. Notably, canopy temperature measured in July-2016 was also positively correlated with the carbon isotope composition ( $\delta^{13}\text{C}$ ) of wood holocellulose for a subset of 25 populations evaluated in the same trial by Voltas et al. (2008, Fig. S2).  $\delta^{13}\text{C}$  is a commonly used integrative indicator of photosynthetic performance, with higher values implying reduced stomatal conductance in the absence of differences in photosynthetic rate (Farquhar et al., 1989). This finding suggests that thermal imagery is indicative of variation in both leaf area and stomatal regulation of gas exchange at the needle level (Gonzalez-Dugo et al., 2013), and is supportive of population differentiation in stomatal conductance in *P. halepensis* during the peak of summer (Voltas et al., 2008).

#### Relationships between vegetation indices and stem volume

Volume over bark (Vob) is a good indicator of above-ground growth in *P. halepensis* as height versus diameter allometry is relatively constant among populations of the species (Vizcaíno-Palomar et al., 2016). However, genetic differences have been described for *P. halepensis* in the allocation of resources to other functions such as reproduction, or to other compartments such as roots (Climent et al., 2008; Cuesta et al., 2010; Voltas et al., 2015). Therefore, population differentiation in Vob could be indicative of either contrasting strategies in resource allocation or superior performance of specific populations showing enhanced growth. We can assume a strong influence of total needle area on Vob as indicated by consistent associations between Vob and NDVI-related indices across populations. This finding indicates that investment in needles is coupled with enhanced above-ground growth in *P. halepensis*, as already reported for other pines (Vose & Allen, 1988; McDowell et al., 2007). Vegetation cover was also correlated with Vob, suggesting complex associations between canopy architecture, canopy density and above-ground growth at the population level.

A negative relation between canopy temperature and Vob among populations was also detected. High canopy temperatures are indicative of decreased transpiration as combination

of reduced leaf area and stomatal conductance (González-Dugo et al., 2013). Since partial correlations between canopy temperature and stem volume were significant after accounting for indices related to leaf area, stomatal regulation is possibly concurring with decreasing transpiring area to limit carbon uptake, leading to reduced growth (Fardusi et al., 2016). Thus, our results suggest that stomatal regulation is a crucial factor accounting for population differentiation in photosynthetic performance of *P. halepensis* under drought conditions. Conversely, low correlations between Vob and pigment-related indices (i.e. TCARI/OSAVI, CRI2 and ARI2) indicate a limited influence of needle phenology and development on population differentiation in above-ground growth.

RGB vegetation indices also showed significant correlations with stem volume, comparable to those obtained from multispectral indices, at least in May-2017. RGB-derived indices have been shown to be good predictors of aerial biomass and yield in crops (Casadesús & Villegas, 2014), in some cases outperforming multispectral indices (Kefauver et al., 2017; Gracia-Romero et al., 2018). Our results show that they can represent a cost-effective alternative to multispectral imagery as a surrogate of above-ground biomass in adult trees. Finally, the outcome of the stepwise regression analyses indicated that a combination of vegetation indices and thermal images can predict up to 60% of population differences in stem volume of adult trees. The best predictive models, involving either RGB and multispectral indices in May-2017, or a combination of a multispectral index and canopy temperature in July-2016, confirmed the concurring role of total leaf area and stomatal regulation in determining stem volume of *P. halepensis*.

#### Methodological limitations

UAVs are increasingly used to characterise genotypic variation in crop trials, which usually consist of isolated plots that are easily recognizable through aerial imagery (Sankaran et al., 2015). In the case of genetic trials of forest species, a high tree density along with heterogeneous trial conditions can hamper the identification of experimental units, especially at adult stages. Moreover, forest trees are characterized by an extreme plasticity in the development of the crown, which can unpredictably grow to exploit the available light (Purves et al., 2007). In aerial imagery, these issues can lead to important disturbances owing to the effects of overlapping crowns of neighbouring plots. We tried to overcome these issues by visually delimiting as carefully as possible crown expansions for each individual plot.

Another potential caveat is related to the existence of unwanted shading effects, which may affect vegetation reflectance and impact on the estimation of indices (Yamazaki et al., 2009). Indeed, phenotypic variation in tree height could lead to systematic shading of some populations. We attempted to minimise this issue by performing flights at noon, but a shading influence on these indices cannot be ruled out, especially in November-2016, when the sun elevation over the horizon was low. In this regard, intricate relationships among indices, weak population differentiation and poor correlations with Vob were observed for this flight date, which suggests that autumn results should be taken cautiously. Finally, another possible limitation towards a precise phenotyping is that UAV-based imagery retrieves information mainly from the top crown of the tree, being less adequate to capture within-crown differences in functional characteristics. These differences are indeed relevant in forest species (Aranda et al., 2004; Yamazaki et al., 2009).

#### Concluding remarks

Plant phenotyping based on UAV remote sensing is coming to an increasing popularity in breeding programs for evaluating and selecting crop varieties for improved yield (Sankaran et al., 2015; Lobos et al., 2017). Here we assessed patterns of genotypic variability in functional traits of adult trees, which is a fundamental step towards the assessment of the adaptive potential of forest species to environmental changes (Bussotti et al., 2015). By using well-established vegetation indices and aerial imagery, our results point to range-wide population differentiation in morphophysiological features related to stem volume in *P. halepensis*, indicating divergent ecophysiological responses and, possibly, changes in resource allocation to growth. This study therefore highlights UAV imagery as a valid high-throughput phenotypic tool with promise to bridge the gap between the molecular and field characterisation of forest tree species, potentially improving the prediction of adaptive responses in the context of global change.

#### Acknowledgments

This work was supported by the Spanish Government [MINECO/FEDER grant number AGL2015-68274-C3-3-R]. We thank the technical assistance of J. del Castillo.

## **Conflict of interest**

The authors declare no conflict of interest

## References

- Aranda I., Pardo F., Gil L., Pardos J. (2004) Anatomical basis of the change in leaf mass per area and nitrogen investment with relative irradiance within the canopy of eight temperate tree species. *Acta Oecologica*, **25**, 187–195.
- Baldwin V.C., Peterson K.D., Burkhart H.E., Amateis R.L., Dougherty P.M. (1997) Equations for estimating loblolly pine branch and foliage weight and surface area distributions. *Canadian Journal of Forest Research*, **27**, 918–927.
- Berni J., Zarco-Tejada P.J., Suarez L., Fereres E. (2009) Thermal and Narrowband Multispectral Remote Sensing for Vegetation Monitoring From an Unmanned Aerial Vehicle. *IEEE Transactions on Geoscience and Remote Sensing*, **47**, 722–738.
- Bussotti F., Pollastrini M., Holland V., Brüggemann W. (2015) Functional traits and adaptive capacity of European forests to climate change. *Environmental and Experimental Botany*, **111**, 91–113.
- Casadesús J., Kaya Y., Bort J., Nachit M.M., Araus J.L., Amor S., Ferrazzano G., Maalouf F., Maccaferri M., Martos V., Ouabbou H., Villegas D. (2007) Using vegetation indices derived from conventional digital cameras as selection criteria for wheat breeding in water-limited environments. *Annals of Applied Biology*, **150**, 227–236.
- Casadesús J., Villegas D. (2014) Conventional digital cameras as a tool for assessing leaf area index and biomass for cereal breeding: Conventional digital cameras for cereal breeding. *Journal of Integrative Plant Biology*, **56**, 7–14.
- Choury Z., Shestakova T.A., Himrane H., Touchan R., Kherchouche D., Camarero J.J., Voltas J. (2017) Quarantining the Sahara desert: growth and water-use efficiency of Aleppo pine in the Algerian Green Barrier. *European Journal of Forest Research*, **136**, 139–152.
- Climent J., Prada M.A., Calama R., Chambel M.R., de Ron D.S., Alia R. (2008) To grow or to seed: ecotypic variation in reproductive allocation and cone production by young female Aleppo pine (*Pinus halepensis*, Pinaceae). *American Journal of Botany*, **95**, 833–842.

Costa J.M., Grant O.M., Chaves M.M. (2013) Thermography to explore plant–environment interactions. *Journal of Experimental Botany*, **64**, 3937–3949.

Cuesta B., Vega J., Villar-Salvador P., Rey-Benayas J.M. (2010) Root growth dynamics of Aleppo pine (*Pinus halepensis* Mill.) seedlings in relation to shoot elongation, plant size and tissue nitrogen concentration. *Trees*, **24**, 899–908.

Daughtry C.S.T., Walthall C.L., Kim M.S., De Colstoun E.B., McMurtrey J.E. (2000) Estimating corn leaf chlorophyll concentration from leaf and canopy reflectance. *Remote sensing of Environment*, **74**, 229–239.

Eamus D., O’Grady A.P., Hutley L. (2000) Dry season conditions determine wet season water use in the wet–tropical savannas of northern Australia. *Tree Physiology*, **20**, 1219–1226.

Fahlgren N., Gehan M.A., Baxter I. (2015) Lights, camera, action: high-throughput plant phenotyping is ready for a close-up. *Current Opinion in Plant Biology*, **24**, 93–99.

Fardusi M.J., Ferrio J.P., Comas C., Voltas J., Resco de Dios V., Serrano L. (2016) Intra-specific association between carbon isotope composition and productivity in woody plants: A meta-analysis. *Plant Science*, **251**, 110–118.

Farquhar G.D., Ehleringer J.R., Hubick K.T. (1989) Carbon Isotope Discrimination and Photosynthesis. *Annual Review of Plant Physiology and Plant Molecular Biology*, **40**, 503–537.

Gitelson A.A., Merzlyak M.N., Chivkunova O.B. (2001) Optical properties and nondestructive estimation of anthocyanin content in plant leaves. *Photochemistry and photobiology*, **74**, 38–45.

Gitelson A.A., Zur Y., Chivkunova O.B., Merzlyak M.N. (2002) Assessing Carotenoid Content in Plant Leaves with Reflectance Spectroscopy. *Photochemistry and photobiology*, **75**, 272–281.

Gonzalez-Dugo V., Zarco-Tejada P., Nicolás E., Nortes P.A., Alarcón J.J., Intrigliolo D.S., Fereres E. (2013) Using high resolution UAV thermal imagery to assess the variability in the water status of five fruit tree species within a commercial orchard. *Precision Agriculture*, **14**, 660–678.

Gracia-Romero A., Kefauver S.C., Vergara-Díaz O., Zaman-Allah M.A., Prasanna B.M., Cairns J.E., Araus J.L. (2017) Comparative Performance of Ground vs. Aerially Assessed RGB and Multispectral Indices for Early-Growth Evaluation of Maize Performance under Phosphorus Fertilization. *Frontiers in Plant Science*, **8**, 2004.

Gracia-Romero A., Vergara-Díaz O., Thierfelder C., Cairns J., Kefauver S., Araus J. (2018) Phenotyping Conservation Agriculture Management Effects on Ground and Aerial Remote Sensing Assessments of Maize Hybrids Performance in Zimbabwe. *Remote Sensing*, **10**, 349.

Großkinsky D.K., Svendsgaard J., Christensen S., Roitsch T. (2015) Plant phenomics and the Need for physiological phenotyping across scales to narrow the genotype-to-phenotype knowledge gap. *Journal of Experimental Botany*, **66**, 5429–5440.

Haboudane D., Miller J.R., Tremblay N., Zarco-Tejada P.J., Dextraze L. (2002) Integrated narrow-band vegetation indices for prediction of crop chlorophyll content for application to precision agriculture. *Remote sensing of environment*, **81**, 416–426.

Hernández-Clemente R., Navarro-Cerrillo R.M., Zarco-Tejada P.J. (2012) Carotenoid content estimation in a heterogeneous conifer forest using narrow-band indices and PROSPECT+ DART simulations. *Remote Sensing of Environment*, **127**, 298–315.

Huete A., Didan K., Miura T., Rodriguez E.P., Gao X., Ferreira L.G. (2002) Overview of the radiometric and biophysical performance of the MODIS vegetation indices. *Remote sensing of environment*, **83**, 195–213.

Hunt E.R., Cavigelli M., Daughtry C.S., McMurtrey J.E., Walthall C.L. (2005) Evaluation of digital photography from model aircraft for remote sensing of crop biomass and nitrogen status. *Precision Agriculture*, **6**, 359–378.

Hunt E.R., Daughtry C.S.T., Eitel J.U.H., Long D.S. (2011) Remote Sensing Leaf Chlorophyll Content Using a Visible Band Index. *Agronomy Journal*, **103**, 1090–1099.

John J.A., Williams E.R. (1998) t-Latinized Designs. *Australian & New Zealand Journal of Statistics*, **40**, 111–118.

Judd D.B. (1940) Hue saturation and lightness of surface colors with chromatic illumination. *Journal of the Optical Society of America*, **30**, 2–32.

Kefauver S.C., Vicente R., Vergara-Díaz O., Fernandez-Gallego J.A., Kerfal S., López A., Melichar J.P.E., Serret M.D., Araus J.L. (2017) Comparative UAV and field phenotyping to assess yield and nitrogen use efficiency in hybrid and conventional barley. *Frontiers in Plant Science*, **8**, 1733.

Klein T. (2014) The variability of stomatal sensitivity to leaf water potential across tree species indicates a continuum between isohydric and anisohydric behaviours. *Functional Ecology*, **28**, 1313–1320.

Klein T., Di Matteo G., Rotenberg E., Cohen S., Yakir D. (2013) Differential ecophysiological response of a major Mediterranean pine species across a climatic gradient. *Tree Physiology*, **33**, 26–36.

Li L., Wu H.X. (2005) Efficiency of early selection for rotation-aged growth and wood density traits in *Pinus radiata*. *Canadian Journal of Forest Research*, **35**, 2019–2029.

Lobos G.A., Camargo A.V., del Pozo A., Araus J.L., Ortiz R., Doonan J.H. (2017) Editorial: Plant Phenotyping and Phenomics for Plant Breeding. *Frontiers in Plant Science*, **8**, 2181.

Ludovisi R., Tauro F., Salvati R., Khoury S., Mugnozza Scarascia G., Harfouche A. (2017) UAV-Based Thermal Imaging for High-Throughput Field Phenotyping of Black Poplar Response to Drought. *Frontiers in Plant Science*, **8**, 1681.

Matyas C. (1996) Climatic adaptation of trees: rediscovering provenance tests. *Euphytica*, **92**, 45–54.

McCrary R.L., Jokela E.J. (1996) Growth phenology and crown structure of selected loblolly pine families planted at two spacings. *Forest Science*, **42**, 46–57.

McDowell N.G., Adams H.D., Bailey J.D., Kolb T.E. (2007) The role of stand density on growth efficiency, leaf area index, and resin flow in southwestern ponderosa pine forests. *Canadian Journal of Forest Research*, **37**, 343–355.

Niinemets Ü. (2010) A review of light interception in plant stands from leaf to canopy in different plant functional types and in species with varying shade tolerance. *Ecological Research*, **25**, 693–714.

Otieno D.O., Schmidt M.W.T., Adiku S., Tenhunen J. (2005) Physiological and morphological responses to water stress in two Acacia species from contrasting habitats. *Tree physiology*, **25**, 361–371.

Otsu N. (1979) A threshold selection method from gray-level histograms. *IEEE transactions on systems, man, and cybernetics*, **9**, 62–66.

Pausas J.G., Bladé C., Valdecantos A., Seva J.P., Fuentes D., Alloza J.A., Vilagrosa A., Bautista S., Cortina J., Vallejo R. (2004) Pines and oaks in the restoration of Mediterranean landscapes of Spain: new perspectives for an old practice—a review. *Plant ecology*, **171**, 209–220.

Peñuelas J., Filella I., Biel C., Serrano L., Save R. (1993) The reflectance at the 950–970 nm region as an indicator of plant water status. *International journal of remote sensing*, **14**, 1887–1905.

Purevdorj T.S., Tateishi R., Ishiyama T., Honda Y. (1998) Relationships between percent vegetation cover and vegetation indices. *International journal of remote sensing*, **19**, 3519–3535.

Purves D.W., Lichstein J.W., Pacala S.W. (2007) Crown Plasticity and Competition for Canopy Space: A New Spatially Implicit Model Parameterized for 250 North American Tree Species. *PLoS ONE*, **2**, e870.

Reinhardt E., Scott J., Gray K., Keane R. (2006) Estimating canopy fuel characteristics in five conifer stands in the western United States using tree and stand measurements. *Canadian Journal of Forest Research*, **36**, 2803–2814.

Richardson A.J., Wiegand C.L. (1977) Distinguishing vegetation from soil background information. *Photogrammetric engineering and remote sensing*, **43**, 1541–1552.

Roberts D.A., Roth K.L., Perroy R.L. (2016) 14 Hyperspectral Vegetation Indices. In *Hyperspectral remote sensing of vegetation*, pp. 309-327. Ed. S.P. Thenkabail, J.G. Lyon. Boca Raton, USA: CRC Press.

Rondeaux G., Steven M., Baret F. (1996) Optimization of soil-adjusted vegetation indices. *Remote sensing of environment*, **55**, 95–107.

Roujean J.L., Breon F.M. (1995) Estimating PAR absorbed by vegetation from bidirectional reflectance measurements. *Remote sensing of Environment*, **51**, 375–384.

Rouse Jr J., Haas R.H., Schell J.A., Deering D.W. (1974) Monitoring vegetation systems in the Great Plains with ERTS. In: *Third ERTS Symposium*, pp. 309-317. Ed. NASA SP-351. Washington DC, USA.

Sankaran S., Khot L.R., Espinoza C.Z., Jarolmasjed S., Sathuvalli V.R., Vandemark G.J., Miklas P.N., Carter A.H., Pumphrey M.O., Knowles N.R., Pavek M.J. (2015) Low-altitude, high-resolution aerial imaging systems for row and field crop phenotyping: A review. *European Journal of Agronomy*, **70**, 112–123.

Santos-del-Blanco L., Bonser S.P., Valladares F., Chambel M.R., Climent J. (2013) Plasticity in reproduction and growth among 52 range-wide populations of a Mediterranean conifer: adaptive responses to environmental stress. *Journal of Evolutionary Biology*, **26**, 1912–1924.

Savolainen O., Pyhäjärvi T., Knürr T. (2007) Gene Flow and Local Adaptation in Trees. *Annual Review of Ecology, Evolution, and Systematics*, **38**, 595–619.

- Schiller G., Atzmon N. (2009) Performance of Aleppo pine (*Pinus halepensis*) provenances grown at the edge of the Negev desert: A review. *Journal of Arid Environments*, **73**, 1051–1057.
- Schindelin J., Arganda-Carreras I., Frise E., Kaynig V., Longair M., Pietzsch T., Preibisch S., Rueden C., Saalfeld S., Schmid B., Tinevez J.Y., White D.J., Hartenstein V., Eliceiri K., Tomancak P., Cardona A. (2012) Fiji: an open-source platform for biological-image analysis. *Nature Methods*, **9**, 676–682.
- Serra-Varela M.J., Alía R., Daniels R.R., Zimmermann N.E., Gonzalo-Jiménez J., Grivet D. (2017) Assessing vulnerability of two Mediterranean conifers to support genetic conservation management in the face of climate change. *Diversity and Distributions*, **23**, 507–516.
- Tang L., Shao G. (2015) Drone remote sensing for forestry research and practices. *Journal of Forestry Research*, **26**, 791–797.
- Tattaris M., Reynolds M.P., Chapman S.C. (2016) A Direct Comparison of Remote Sensing Approaches for High-Throughput Phenotyping in Plant Breeding. *Frontiers in Plant Science*, **7**, 1131.
- Tognetti R., Michelozzi M., Giovannelli A. (1997) Geographical variation in water relations, hydraulic architecture and terpene composition of Aleppo pine seedlings from Italian provinces. *Tree Physiology*, **17**, 241–250.
- Torresan C., Berton A., Carotenuto F., Di Gennaro S.F., Gioli B., Matese A., Miglietta F., Vagnoli C., Zaldei A., Wallace L. (2017) Forestry applications of UAVs in Europe: A review. *International Journal of Remote Sensing*, **38**, 2427–2447.
- Vizcaíno-Palomar N., Ibáñez I., González-Martínez S.C., Zavala M.A., Alía R. (2016) Adaptation and plasticity in aboveground allometry variation of four pine species along environmental gradients. *Ecology and Evolution*, **6**, 7561–7573.

- Voltas J., Chambel M.R., Prada M.A., Ferrio J.P. (2008) Climate-related variability in carbon and oxygen stable isotopes among populations of Aleppo pine grown in common-garden tests. *Trees*, **22**, 759–769.
- Voltas J., Lucabaugh D., Chambel M.R., Ferrio J.P. (2015) Intraspecific variation in the use of water sources by the circum-Mediterranean conifer *Pinus halepensis*. *New Phytologist*, **208**, 1031–1041.
- Voltas J., Shestakova, T.A., Patsiou, T., di Matteo, G., Klein, T. (2018) Ecotypic variation and stability in growth performance of the thermophilic conifer *Pinus halepensis* across the Mediterranean basin. *Forest Ecology and Management*, **424**, 205–215.
- Vose J.M., Allen H.L. (1988) Leaf area, stemwood growth, and nutrition relationships in loblolly pine. *Forest Science*, **34**, 547–563.
- Weinstein A. (1989) Geographic variation and phenology of *Pinus halepensis*, *P. brutia* and *P. eldarica* in Israel. *Forest Ecology and Management*, **27**, 99–108.
- Weiskittel A.R., Maguire D.A. (2006) Branch surface area and its vertical distribution in coastal Douglas-fir. *Trees*, **20**, 657–667.
- Wong C.Y.S., Gamon J.A. (2015) The photochemical reflectance index provides an optical indicator of spring photosynthetic activation in evergreen conifers. *New Phytologist*, **206**, 196–208.
- Wu C., Niu Z., Tang Q., Huang W. (2008) Estimating chlorophyll content from hyperspectral vegetation indices: Modeling and validation. *Agricultural and Forest Meteorology*, **148**, 1230–1241.
- Xue J., Su B. (2017) Significant Remote Sensing Vegetation Indices: A Review of Developments and Applications. *Journal of Sensors*, **2017**, 1–17.

Yamazaki F., Liu W., Takasaki M. (2009) Characteristics of shadow and removal of its effects for remote sensing imagery, In: *Geoscience and Remote Sensing Symposium, IEEE*, pp. IV–426. Ed. IEEE International, IGARSS.

Yu N., Li L., Schmitz N., Tian L.F., Greenberg J.A., Diers B.W. (2016) Development of methods to improve soybean yield estimation and predict plant maturity with an unmanned aerial vehicle based platform. *Remote Sensing of Environment*, **187**, 91–101.

Zarco-Tejada P., Miller J., Morales A., Berjón A., Agüera J. (2004) Hyperspectral indices and model simulation for chlorophyll estimation in open-canopy tree crops. *Remote Sensing of Environment*, **90**, 463–476.

## **Supporting Information**

**Table S1.** Geographic origin of the 56 *Pinus halepensis* populations tested in the trial.

**Table S2.** Average values and standard deviation of vegetation indices, vegetation cover and canopy temperature in July-2016, November-2016 and May-2017.

**Table S3.** Spearman's rank correlations between population means of VIs across flights.

**Table S4.** Association between RGB and multispectral indices in July-2016.

**Table S5.** Association between RGB and multispectral indices in November-2016.

**Table S6.** Association between RGB and multispectral indices in May-2017.

**Fig. S1.** Map of the origin of the 56 *Pinus halepensis* populations tested in the trial.

**Fig. S2.** Association between canopy temperature in July-2016 and carbon isotope composition of wood holocellulose reported in Voltas et al. (2008)

**Table 1.** Environmental and sun conditions at the moment of each flight. Air temperature (T) and relative humidity (RH) were measured in situ and used to estimate vapour pressure deficit (VPD). Azimut and sun elevation were calculated based on the position of the trial, the period of the year and the time of the flight. Sun radiation was retrieved for the time of the flight from a meteorological station located *ca.* 10 km away from the trial.

<b>Variable</b>	<b>July 2016</b>	<b>Nov. 2016</b>	<b>May 2017</b>
T (°C)	33.2	18.6	32.2
RH (%)	38.8	37.3	23.0
VPD (kPa)	3.1	1.3	3.7
Azimut (°)	225	207	232
Sun elevation (°)	62.8	26.3	63.0
Sun radiation (W m <sup>-2</sup> )	846	527	863

**Table 2.** Multispectral and RGB-derived vegetation indices (VIs) considered in this study. For those indices based on specific bands of the light spectrum, the formula used for calculation is reported. R indicates the reflectance in a single or in a range of wavelengths (in nm). RGB indices were calculated considering a continuous range of wavelengths, while single bands were used for multispectral VIs. The calculation of other indices that are not based on the reflectance in specific bands (Intensity, Hue, Saturation, a\*, b\*, u\*, v\* and GA) is described in the text.

Index	Descriptor	Wavelengths	Formula	Reference
<b>Multispectral VIs</b>				
NDVI	Leaf area	Red, NIR	$(R_{840} - R_{670}) / (R_{840} + R_{670})$	Rouse et al., 1973
OSAVI	Leaf area	Red, NIR	$(R_{840} - R_{670}) / (R_{840} + R_{670} + 0.16) \times 1.16$	Rondeaux et al., 1996
RDVI	Leaf area	Red, NIR	$(R_{840} - R_{670}) / (R_{840} + R_{670})^{1/2}$	Roujean & Breon, 1995
EVI	Leaf area	Blue, Red, NIR	$2.5 \times (R_{840} - R_{670}) / [(R_{840} + 6 \times R_{670} - 7.5 \times R_{450}) + 1]$	Huete et al., 2002
MCARI	Leaf chlorophyll content; leaf area	Green, Red, NIR	$[(R_{700} - R_{670}) - 0.2 \times (R_{700} - R_{550})] \times (R_{700} / R_{670})$	Daughtry, 2000
TCARI	Leaf chlorophyll content; leaf area	Green, Red, NIR	$3 \times (R_{700} - R_{670}) - 0.2 \times (R_{700} - R_{550}) \times (R_{700} / R_{670})$	Haboudane et al., 2002
TCARI/OSAVI	Leaf chlorophyll content	Green, Red, NIR	-	Haboudane et al., 2002
ARI2	Anthocyanins content	Blue, NIR	$R_{840} \times (1/R_{550} - 1/R_{700})$	Gitelson et al., 2001
CRI2	Carotenoid content	Blue, NIR	$1/R_{550} - 1/R_{700}$	Gitelson et al., 2002
WBI	Water content	NIR	$R_{900} / R_{950}$	Peñuelas et al., 1993
<b>RGB VIs</b>				
NRGDI	Leaf area	Green, Red	$(R_{490:570} - R_{640:760}) / (R_{490:570} + R_{640:760})$	Hunt et al., 2005
TGI	Leaf chlorophyll content	Green, Red, Blue	$-0.5 \times [(R_{665:675} - R_{475:485}) \times (R_{670} - R_{550}) - (R_{665:675} - R_{445:555}) \times (R_{670} - R_{480})]$	Hunt et al., 2011
Intensity	-	Visible spectrum	-	Casadesús et al., 2007
Hue	-	Visible spectrum	-	Casadesús et al., 2007
Saturation	-	Visible spectrum	-	Casadesús et al., 2007
a*	-	Visible spectrum	-	Casadesús et al., 2007
b*	-	Visible spectrum	-	Casadesús et al., 2007
u*	-	Visible spectrum	-	Casadesús et al., 2007
v*	-	Visible spectrum	-	Casadesús et al., 2007
GA	-	Visible spectrum	-	Casadesús et al., 2007

**Table 3.** *F* statistics and *P* values of the fixed population effect of the ANOVA fitted for each vegetation index and flight.

		July 2016		Nov. 2016		May 2017	
		<i>F</i>	<i>P</i> - value	<i>F</i>	<i>P</i> - value	<i>F</i>	<i>P</i> - value
<b>Multispectral VIs (plot)</b>							
	<b>NDVI</b>	1.16	0.25	1.51	0.03	1.39	0.07
	<b>OSAVI</b>	1.68	0.01	1.49	0.04	1.77	<0.01
	<b>RDVI</b>	1.74	<0.01	1.59	0.02	1.91	<0.01
	<b>EVI</b>	1.83	<0.01	1.28	0.13	0.85	0.74
	<b>MCARI</b>	2.16	<0.01	1.74	<0.01	2.88	<0.01
	<b>TCARI</b>	1.86	<0.01	1.44	0.05	2.29	<0.01
	<b>TCARI/OSAVI</b>	1.20	0.21	1.00	0.48	1.27	0.13
	<b>ARI2</b>	1.67	0.01	1.30	0.11	1.69	<0.01
	<b>CRI2</b>	1.45	0.05	1.20	0.21	1.35	0.09
	<b>WBI</b>	1.21	0.19	1.12	0.30	1.97	<0.01
<b>Multispectral VIs (vegetation)</b>							
	<b>NDVI</b>	1.68	0.01	1.99	<0.01	1.75	<0.01
	<b>OSAVI</b>	2.61	<0.01	1.88	<0.01	2.41	<0.01
	<b>RDVI</b>	2.72	<0.01	1.95	<0.01	2.60	<0.01
	<b>EVI</b>	2.36	<0.01	1.93	<0.01	2.43	<0.01
	<b>MCARI</b>	3.26	<0.01	2.01	<0.01	3.48	<0.01
	<b>TCARI</b>	2.27	<0.01	1.47	0.04	2.38	<0.01
	<b>TCARI/OSAVI</b>	1.20	0.21	1.22	0.18	1.48	0.04
	<b>ARI2</b>	1.33	0.10	1.01	0.47	1.86	<0.01
	<b>CRI2</b>	1.12	0.29	1.05	0.41	1.69	<0.01
	<b>WBI</b>	1.05	0.39	1.07	0.36	2.35	<0.01
<b>RGB VIs</b>							
	<b>NGRDI</b>	1.89	<0.01	1.34	0.09	1.87	<0.01
	<b>TGI</b>	1.16	0.24	0.22	0.88	1.46	0.05
	<b>Intensity</b>	1.15	0.25	0.26	0.81	1.47	0.04
	<b>Hue</b>	1.96	<0.01	0.12	1.30	1.43	0.05
	<b>Saturation</b>	1.73	<0.01	1.34	0.09	2.01	<0.01
	<b>a*</b>	1.91	<0.01	1.59	0.02	2.35	<0.01
	<b>b*</b>	1.46	0.04	1.24	0.16	2.10	<0.01
	<b>u*</b>	1.61	0.02	1.53	0.03	2.30	<0.01
	<b>v*</b>	1.39	0.07	1.25	0.15	2.12	<0.01
	<b>GA</b>	2.25	<0.01	1.85	<0.01	2.25	<0.01
<b>Vegetation cover</b>							
		1.78	<0.01	1.56	0.02	1.49	0.04
<b>Canopy temperature*</b>							
		1.54	0.03	1.01	0.47	0.92	0.63

\* only pixels classified as “vegetation” in July-2016 and May-2017; whole-plot temperature (all pixels) in November-2016.

**Table 4.** Pearson correlation coefficients between population means of vegetation indices (VI) and either vegetation cover (VC) or log-transformed stem volume (Vob). Empty cells indicate lack of population differentiation for the corresponding VI as found in the ANOVAs.

	VC			Vob		
	July 16	Nov. 2016	May 2017	July 16	Nov. 2016	May 2017
<b>Multispectral VIs (plot)</b>						
NDVI	-	0.47**	-	-	0.35**	-
OSAVI	0.65**	0.63**	0.72**	0.68**	0.62**	0.59**
RDVI	0.62**	0.64**	0.72**	0.69**	0.60**	0.57**
EVI	0.54**	-	-	0.66**	-	-
MCARI	0.44**	0.55**	0.52**	0.65**	0.54**	0.35**
TCARI	0.43**	0.64**	0.34*	0.58**	0.57**	0.17
TCARI/OSAVI	-	-	-	-	-	-
ARI2	-	-	-0.31*	-	-	-0.03
CRI2	-0.32*	-	-0.41**	-0.35**	-	-0.10
WBI	-	-	-0.28*	-	-	-0.19
<b>Multispectral VIs (vegetation)</b>						
NDVI	0.23	0.20	0.54**	0.52**	0.41**	0.60**
OSAVI	0.33*	0.26	0.60**	0.69**	0.63**	0.58**
RDVI	0.30*	0.23	0.58**	0.69**	0.65**	0.57**
EVI	0.34*	0.28*	0.44**	0.70**	0.65**	0.39**
MCARI	0.13	0.24	0.31*	0.60**	0.57**	0.28*
TCARI	0.21	0.28*	0.22	0.62**	0.66**	0.16
TCARI/OSAVI	-	-	-0.26	-	-	-0.35**
ARI2	-	-	-0.07	-	-	0.02
CRI2	-	-	-0.32*	-	-	-0.12
WBI	-	-	-0.39**	-	-	-0.30*
<b>RGB VIs</b>						
NGRDI	0.57**	-	0.71**	0.47**	-	0.59**
TGI	-	-	-0.44**	-	-	-0.60**
Intensity	-	-	-0.45**	-	-	-0.62**
Hue	0.59**	-	0.05	0.53**	-	0.00
Saturation	0.48**	-	0.59**	0.60**	-	0.57**
a*	-0.60**	-0.50**	-0.66**	-0.51**	-0.56**	-0.49**
b*	0.55**	-	0.62**	0.53**	-	0.48**
u*	-0.52**	-0.46**	-0.62**	-0.44**	-0.37**	-0.44**
v*	-	-	0.62**	-	-	0.42**
GA	0.37**	0.53**	0.68**	0.51**	0.46**	0.49**

Significant correlations are indicated by \* ( $P < 0.05$ ) or \*\* ( $P < 0.01$ )

**Table 5.** Stepwise multiple linear regression of stem volume (log-transformed) based on the different categories of vegetation indices (multispectral on the whole plot [Multispectral <sub>p</sub>], multispectral on pixels containing vegetation [Multispectral <sub>v</sub>], or RGB-derived) in July-2016 and May-2017. RGB indices were also combined with the two groups of multispectral indices. Only the combination showing the highest R<sup>2</sup> (with either multispectral indices measured on the whole plot or on pixels containing vegetation) is reported.

	<b>Indices categories</b>	<b>Model</b>	<b>R<sup>2</sup></b>	<b>RMSE</b>
<b>July 2016<sup>a</sup></b>	<b>Multispectral <sub>p</sub></b>	$\text{Log}(\text{Vob}) = 14.44 \times \text{OSAVI} - 2.85$	0.48	0.311
	<b>Multispectral <sub>v</sub></b>	$\text{Log}(\text{Vob}) = 7.02 \times \text{OSAVI} + 4.68 \times \text{EVI} + 0.02 \times \text{VC} - 4.09$	0.50	0.314
	<b>RGB</b>	$\text{Log}(\text{Vob}) = 15.49 \times \text{Saturation} - 1.87$	0.35	0.353
	<b>RGB + Multispectral <sub>p</sub></b>	$\text{Log}(\text{Vob}) = 9.88 \times \text{Saturation} + 0.30 \times u^* + 18.09 \times \text{OSAVI} - 8.35$	0.57	0.292
<b>July 2016 - T<sup>b</sup></b>	<b>Multispectral <sub>p</sub></b>	$\text{Log}(\text{Vob}) = 6.09 \times \text{OSAVI} - 0.38 \times \text{T} + 12.88$	0.61	0.276
	<b>Multispectral <sub>v</sub></b>	$\text{Log}(\text{Vob}) = 3.90 \times \text{EVI} - 0.40 \times \text{T} + 14.06$	0.60	0.278
	<b>RGB</b>	$\text{Log}(\text{Vob}) = -0.53 \times \text{T} + 20.30$	0.57	0.287
	<b>RGB + Multispectral <sub>v</sub></b>	$\text{Log}(\text{Vob}) = 3.90 \times \text{EVI} - 0.40 \times \text{T} + 14.06$	0.60	0.278
<b>May 2017</b>	<b>Multispectral <sub>p</sub></b>	$\text{Log}(\text{Vob}) = 19.11 \times \text{OSAVI} - 15.82 \times \text{MCARI} + 3.49 - 3.23$	0.40	0.241
	<b>Multispectral <sub>v</sub></b>	$\text{Log}(\text{Vob}) = 12.80 \times \text{NDVI} + 5.21 \times \text{EVI} - 11.09 \times \text{MCARI} - 7.59$	0.46	0.235
	<b>RGB</b>	$\text{Log}(\text{Vob}) = 0.77 \times \text{NGRDI} - 4.12 \times \text{Intensity} + 0.57 \times b^* - 1.55 \times v^* - 6.15$	0.57	0.210
	<b>RGB + Multispectral <sub>v</sub></b>	$\text{Log}(\text{Vob}) = 0.71 \times \text{NGRDI} - 5.98 \times \text{Intensity} + 0.60 \times b^* - 0.69 \times v^* + 2.43 \times \text{GA} + 11.93 \times \text{MCARI} + 6.88$	0.63	0.198

<sup>a</sup> regression performed without considering canopy temperature; <sup>b</sup> regression including canopy temperature

## Figure legends

**Figure 1** Aerial images of the genetic trial of *P. halepensis* considered for this study and main characteristics of the 56 populations tested. A) Aerial image of the complete trial; the black line represents the approximate trajectory followed by the UAV. B) Mean annual precipitation ( $P_{an}$ ) and temperature ( $T_{an}$ ) for the distribution range (EUFORGEN distribution map (<http://www.euforgen.org/species/pinus-halepensis/>) of *P. halepensis* (grey dots) calculated in 10' resolution grids from the WorldClim database (period 1960-1990). Temperature and precipitation of the site where the 56 populations were located at origin (black dots) and of the trial site (red dot) are shown. C) Aerial image of one experimental unit in RGB. D) Aerial image of one experimental unit as in C) in infrared (false colour). E) Aerial image of one experimental unit as in C) in infrared, but cropped for pixels containing vegetation ( $NDVI > 0.5$ ).

**Figure 2** Component loadings of the Principal Component Analysis for multispectral indices measured on whole plot (A), multispectral indices measured on vegetation pixels only (B) and of RGB-derived indices (C) plus canopy temperature (T) measured in July-2016 based on population means. Abbreviations are as reported in the “Material and Methods” section.

**Figure 3** Correlation between canopy temperature (measured on pixels containing vegetation) and stem volume (log-transformed) calculated at the population level in July-2016. Codes represent the populations tested in the trial as in Supporting Information (Table S1).

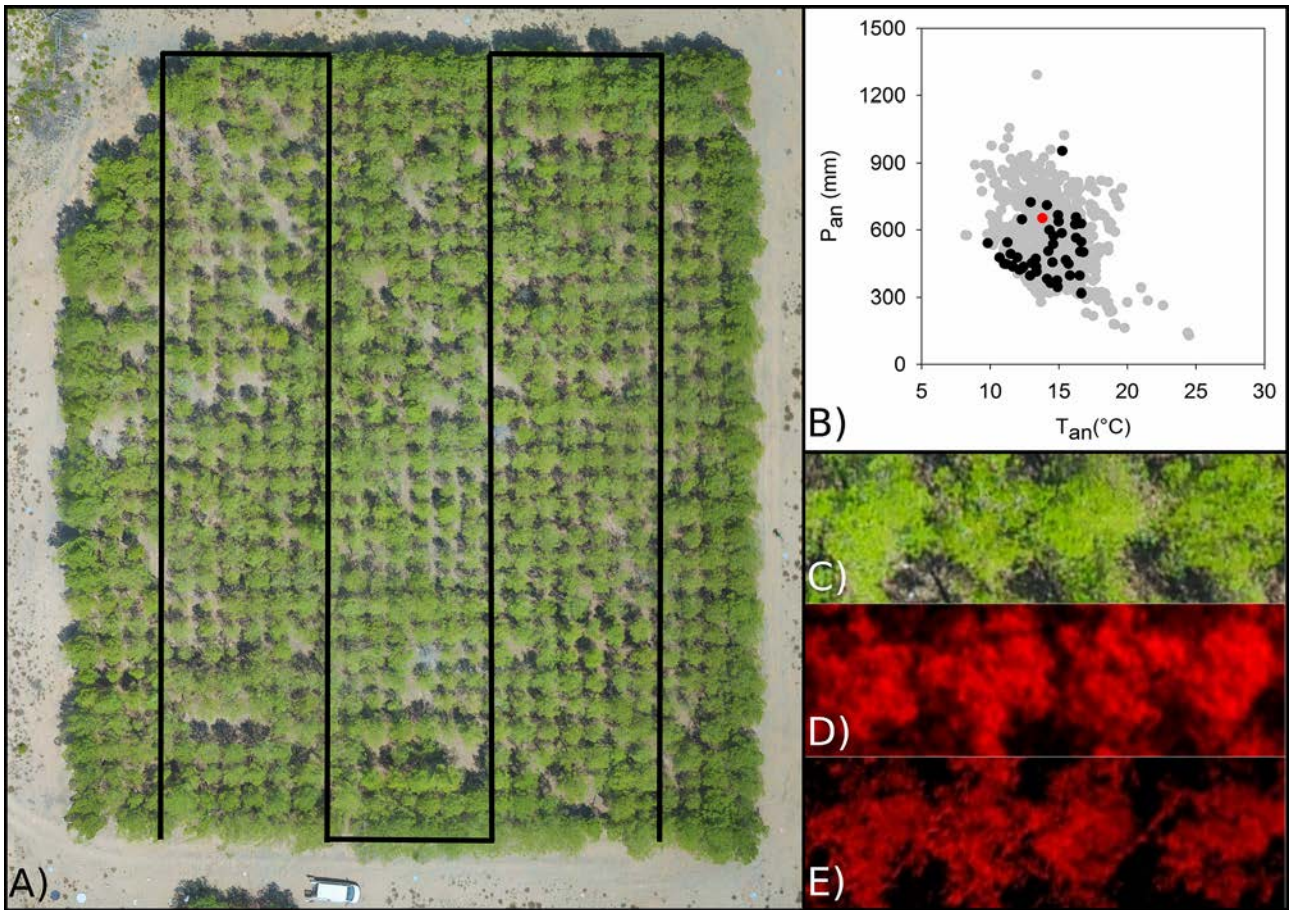
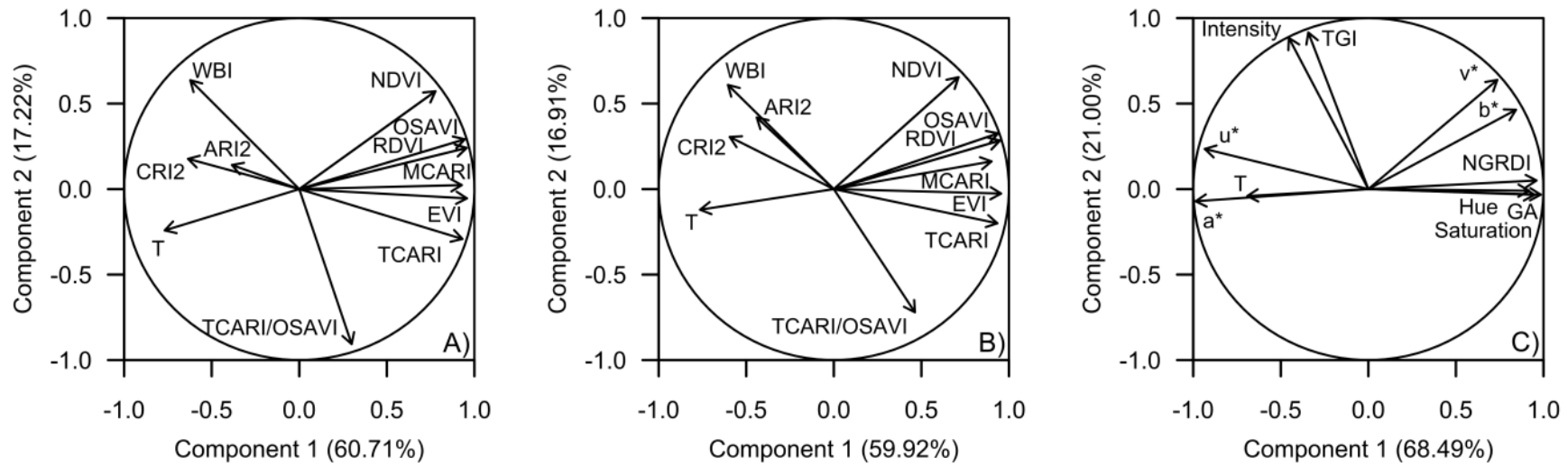
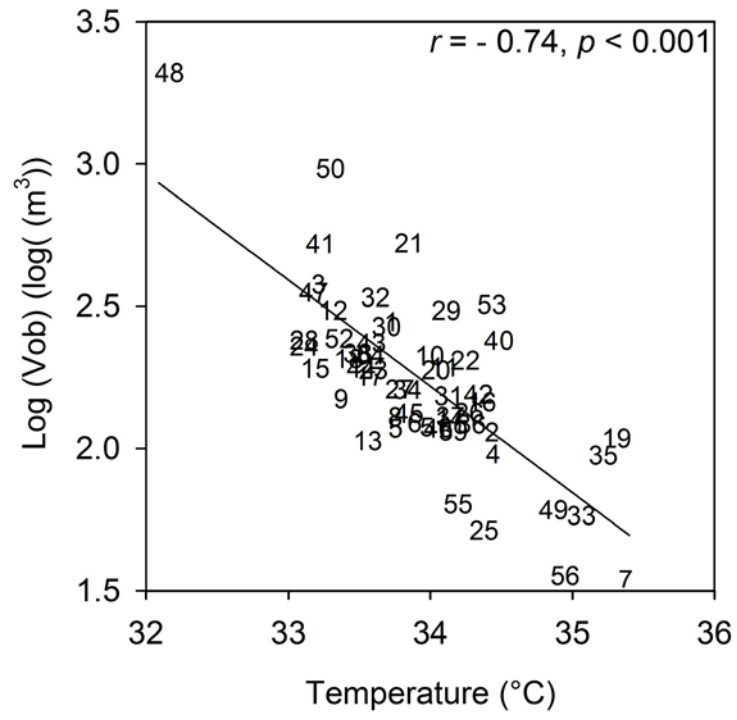


Figure 1 (Online colour only)



**Figure 2**



**Figure 3**